DOE/SC-ASR-15-001

Addressing Numerical Challenges Associated with Large-Eddy Simulations using the Weather Research and Forecasting Model

Jerome D. Fast
Heng Xiao
William I. Gustafson Jr.
May Wong
Wuyin Lin
Andrew Vogelmann
Satoshi Endo
Hailong Wang
Yangang Liu

March 2015

U.S. DEPARTMENT OF
ENERGY
Office of Science

ASR
Atmospheric
System Research

DISCLAIMER

DOE/SC-ASR-15-001

Addressing Numerical Challenges Associated with Large-Eddy Simulations using the Weather Research and Forecasting Model

Jerome D. Fast
Heng Xiao
William I. Gustafson Jr.
May Wong
Wuyin Lin
Andrew Vogelmann
Satoshi Endo
Hailong Wang
Yangang Liu

March 2015

Work supported by the U.S. Department of Energy,
Office of Science, Office of Biological and Environmental Research

Executive Summary

Large-eddy simulation (LES) modeling is useful for better understanding specific processes associated with the planetary boundary layer, clouds, aerosols, and cloud-aerosol interactions. While the scientific community has benefited from many LES case studies, routine use of LES coupled with high-resolution meteorology, radiation, and cloud property measurements from the United States Department of Energy (DOE) Atmospheric Radiation Measurement (ARM) "megasites" has the potential to dramatically improve process-level understanding and improve climate model parameterizations. A number of LES models could potentially be used routinely at the ARM Southern Great Plains (SGP) site. One option is the community-developed Weather Research and Forecasting (WRF) model that solves the fully compressible equations, as opposed to LES models that use less computationally expensive approximations. Unfortunately, Yamaguchi and Feingold (2012; hereafter YF12) identified a susceptibility to time-step convergence sensitivity in WRF for LES simulations. The goals of this study are to (1) investigate the concerns associated with the convergence issue and (2) to provide solutions.

Through a series of sensitivity simulations based on the marine conditions examined in YF12 plus cases at the ARM SGP site, we found that the convergence issue (i.e., time-step dependency) noted by YF12 results from numerical instability with respect to propagating acoustic waves when solving the fully compressible equations. It occurs when a large specific humidity jump exists across the inversion at the top of the boundary layer combined with sufficiently strong wind speed. The numerical noise stabilizes sufficiently such that it does not cause simulations to crash, but it does lead to errant enhanced vertical mixing at the top of the inversion and reductions in cloud amount. Long-term measurements from the ARM Planetary Boundary Layer Value-Added Product show that meteorological conditions predisposing WRF to exhibit the convergence issue potentially occur ~8% of the year, on average. A shortened model time step prevents the errant cloud behavior, but a time step short enough to cover all possible meteorological conditions is computationally expensive, so other solutions are sought.

Our team tested two mitigating methodologies for the convergence issue. (1) Using a Galilean transformation of the domain that reduces noise generation by slowing the relative wind speed at the boundary-layer top where the numerical noise occurs. (2) Using the weighted essentially non-oscillatory (WENO) advection scheme in WRF combined with increased divergence damping, which inhibits the generation of spurious small oscillations along strong gradients and minimizes the numerical noise that leads to the convergence issue. Both methods can effectively mask the issue, but still require users to carefully examine their solutions to ensure convergence has been achieved.

The best solution is to remove the convergence issue, which can be achieved through a minor reformulation of the WRF dynamical core. A careful examination of the numerics identified an inconsistency in how potential temperature and moisture are handled during acoustic sub-stepping. In partnership with the dynamical core developers we modified WRF to consistently use water vapor throughout the acoustic sub-steps, which resulted in removing the convergence issue. We have verified that the convergence issue no longer exists in our test cases. And, there is the added computational benefit that the modification enables longer time steps at LES scales. The improved dynamical core is slated for release in WRF v3.7 in spring 2015, at which point it will be publically available to the community. Based on results with the improved dynamical core we conclude that the numerical issues identified in YF12 should not be a factor when considering using WRF for routine LES applications at the SGP site.

Acknowledgments

We thank Bill Skamarock, Joe Klemp, and Branko Kosovic (National Center for Atmospheric Research) for taking time to investigate the numerical issues associated with the dynamical core in the WRF model as well as their helpful suggestions to fix the problem.

Acronyms and Abbreviations

ARM	Atmospheric Radiation Measurement
ARMBE	ARM Best Estimate
ARSCL	Active Remotely Sensed Cloud Locations
CFL	Courant-Friedrichs-Lewy
ENO	Essentially Non-Oscillatory
LES	Large-eddy simulation
LWP	Liquid water path
NCAR	National Center for Atmospheric Research
PBL	Planetary Boundary Layer
SCM	Single Column Model
SGP	Southern Great Plains
TSI	Total-sky imager
VAP	Value-Added Product
WENO	Weighted essentially non-oscillatory
WRF	Weather Research and Forecasting

Contents

Figures

1.0 Introduction

1.1 Background

Large-eddy simulation (LES) models are useful tools to study planetary boundary layers, aerosols, clouds, and cloud-aerosol interactions. While the field has benefited from many LES case studies, routine use of LES, coupled with the high-resolution meteorology, radiation, and cloud property measurements at ARM "megasites," has the potential to dramatically improve process understanding and constraints for climate model parameterizations. High-resolution modeling also provides estimates of spatiotemporally varying cloud microphysical and atmospheric turbulence properties, filling in details that may not be sampled by the ARM observations. There are a number of LES models that could be potentially used routinely at the ARM SGP site. The Weather Research and Forecasting (WRF) community model is one candidate whose performance is similar to other LES models (e.g., Moeng et al. 2007; Wang et al. 2009; Blossey et al. 2013; Ovchinnikov et al. 2014; Xiao et al. 2014; and Endo et al. 2015). The community model approach has led to the availability of multiple options for each physics parameterization and easily accommodates their continual improvement through regular release updates. WRF has the capability of running two-way multiple nested grids, enabling realistic temporally and spatially varying boundary conditions for the LES domain and interactions between turbulent motions and mesoscale systems. Several data assimilation packages have already been developed that could be used to merge ARM data with the WRF simulation to produce high-resolution analyses over the SGP site. In addition, treatments of the aerosol life cycle have been implemented that enable a more realistic representation of cloud-aerosol interactions.

However, unlike many other LES models, WRF solves a fully compressible system of equations for the atmosphere, as opposed to using an incompressible approach or using the anelastic approximation that is computationally efficient but can be violated under certain convective conditions. Yamaguchi and Feingold (2012; hereafter YF12) showed for three idealized cases (DYCOMS-II RF01, Stevens et al. 2005; DYCOMS-II RF02, Ackerman et al. 2009; and RICO, van Zantel et al. 2011) that WRF LESs can be susceptible to time-step convergence sensitivity, which we show results from numerical instability with respect to propagating acoustic waves when solving the fully compressible equations. We reproduced the convergence (or time-step dependency) issue raised by YF12 for DYCOMS-II RF02 as shown in Figure 1. The WRF simulations are in reasonable agreement with the range of liquid water path (LWP) simulated by various LES models (shaded gray, from Ackerman et al. 2009) when either the model time step for dynamics and physics is small ($\Delta t = 0.25$ s) or the number of acoustic time steps, N_{aco}, within Δt is large ($N_{aco} = 12$). In contrast, the LWP from the simulation that uses $\Delta t = 0.5$ s and $N_{aco} = 6$ is significantly smaller and indicative of the convergence issue raised by YF12.

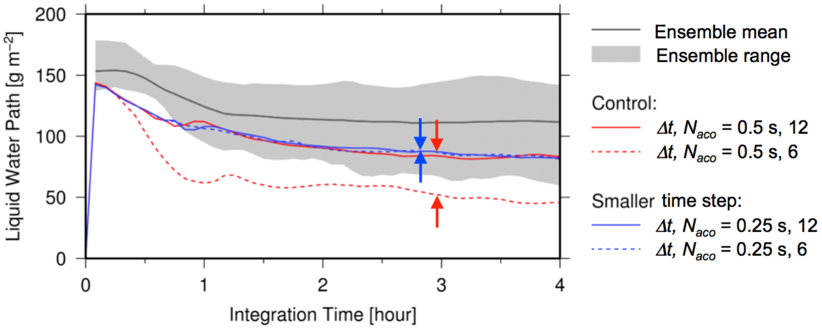

Figure 1. The time-step dependency issue recreated from the DYCOMS-II RF02 case for precipitating marine stratocumulus clouds (colored lines). The ensemble mean (black line) and range (shaded) are from eight LES models in Ackerman et al. (2009). The arrows highlight the non-converged state of the control simulation (red) compared to using a smaller time step (blue).

1.2 Objectives

In this study, we focus on the feasibility of using WRF at LES scales for shallow cloud conditions. The primary goals of this study are to:

- investigate the convergence issue for WRF at LES scales, and
- provide candidate solutions.

We assess the impact of the issue on the simulation of clouds for the wide range of realistic atmospheric conditions at SGP and identify the cause of the issue, which was not addressed by YF12.

2.0 Results

The following describes how we addressed the convergence issue in WRF at LES scales, an analysis of how the convergence issue could impact LES simulations at the SGP site, and our proposed approaches for avoiding the issue. We first reproduce the convergence issue described in YF12 for the DYCOMS-II RF02 case (Ackerman et al. 2009; hereafter called the DRF02 case), and then use this case to perform sensitivity simulations to identify factors that predispose WRF to the convergence issue. Additional simulations were performed using SGP observations as initial conditions to confirm that the issue can occur for shallow cloud conditions over land in addition to the maritime conditions of DRF02. A method was developed to detect the numerical noise issue early in the simulations, which is used to determine a 2D parameter space of problematic environmental conditions. We then examine the SGP climatology to identify the frequency of meteorological conditions conducive to the convergence issue. Methods developed to detect the numerical noise are presented to enable users to identify the issue early in their simulations. Finally, we present three approaches that mitigate or entirely eliminate the numerical noise that ultimately causes the convergence issue. We describe the strengths and weaknesses of each approach and recommend the best option for WRF LES, such as routine operations at ARM sites.

2.1 Understanding the Conditions Conducive to Convergence Issues in WRF

DRF02 case: We first explored the convergence issue shown in Figure 1 using the DRF02 case. Specifically, we quantified the dependence of the issue on the meteorological state and for pairings of the number of acoustic sub-steps, N_{aco}, per model dynamics time step, Δt, when using a grid spacing of 50 m. The model configuration follows the DRF02 description in Ackerman et al. (2009) with specifics regarding the WRF configuration given in Appendix A. The results for various N_{aco} settings for $\Delta t = 0.5$ s are given in Figure 2, which shows the time variations of LWP, cloud-base and cloud-top height, and total cloud fraction. The results for simulations with $N_{aco} = 12$ and 15 are in close agreement for all four cloud variables, indicating a converged solution, while $N_{aco} = 6$ is markedly different, particularly in terms of LWP and total cloud fraction. The cloud variables for $N_{aco} = 9$ are very similar to the converged values. Thus, for the discussions that follow, results emphasize $N_{aco} = 12$ and 6, respectively representing the converged and non-converged solutions.

The vertical profiles of meteorological variables from simulations using different acoustic sub-step counts are depicted in Figure 3. Similar to the time-series results (Figures 1 and 2), the simulation using $N_{aco} = 6$ does not converge with other simulations. Compared to the converged simulations, the $N_{aco} = 6$ simulation has smoother vertical variations in potential temperature and water vapor mixing ratio above the inversion, smaller liquid water mixing ratio and cloud fraction, and smoother horizontal wind variations near the inversion. The profiles of turbulence characteristics, such as variance and covariance, also have similar changes around the inversion and in the cloud layer (not shown). These results demonstrate the convergence issue is associated with factors associated with the inversion.

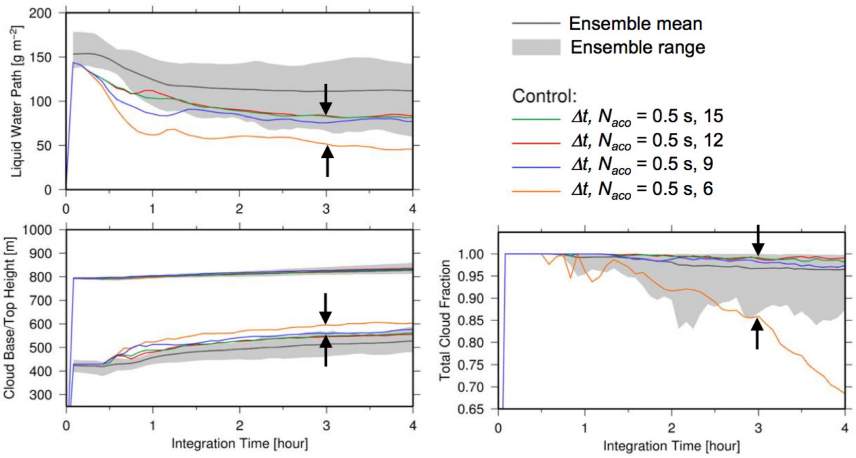

Figure 2. Time series of LWP, cloud-top and cloud-base heights, and cloud fraction from DRF02 simulations using Δt = 0.5 s and N_{aco} = 6, 9, 12, and 15. Following Ackermann et al. (2009), cloud-top is defined as the height of domain-averaged total water = 8 g kg^{1} and cloud fraction is defined as domain fraction of columns with column LWP > 20 g m^{-2}. The arrows indicate the range of variability in WRF results due to non-convergence.

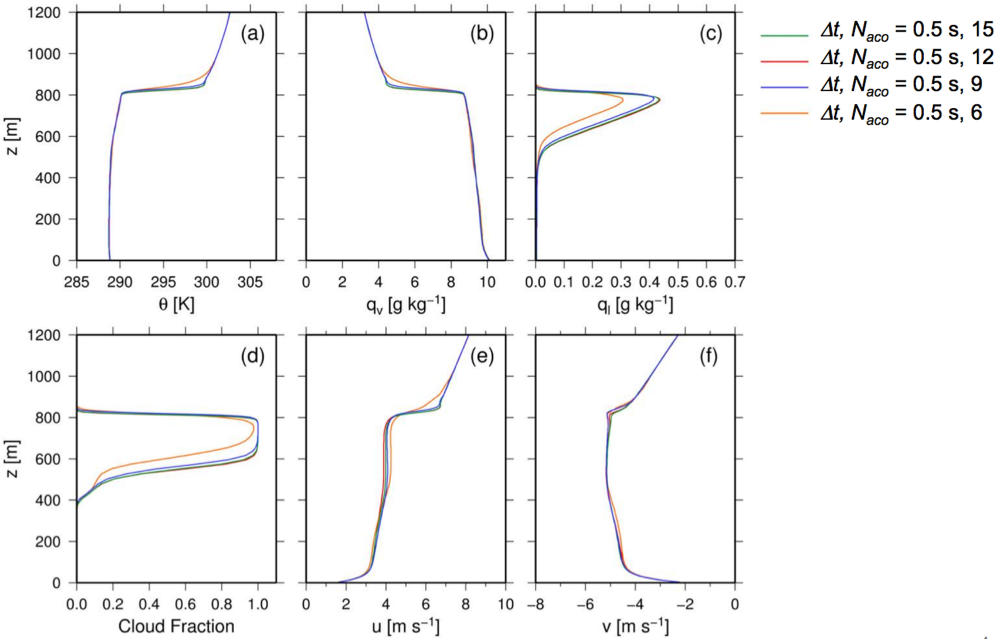

Figure 3. Vertical profiles of potential temperature (θ), water vapor mixing ratio (q_v), liquid water mixing ratio (q_l), cloud fraction, and horizontal wind components (u, v). Values are averages for hours 2 to 4 of the integration period for DRF02 simulations using N_{aco} = 6, 9, 12, and 15.

Numerous sensitivity studies and analyses were performed on the DRF02 case to identify conditions and factors associated with the convergence issue. The analyses facilitate basic understanding of the problem, and the findings were used to identify potentially problematic meteorological conditions at the ARM SGP site. We examined more than 200 simulations to test different initial conditions, surface and large-scale forcings, physics package selections, dynamics options, and vertical grid settings. The two key findings described are that the acoustic time-step dependency appears to be associated with the wind speed (not shear) and moisture gradient, both at the inversion height.

Over time, the sensitivity of LWP to changes in the initial wind profiles at the inversion height is given in Figure 4. In the initial wind profile of the DRF02 case, *u* and *v* change linearly with height. We modified the initial horizontal wind for three sensitivity tests such that the winds are:

1. zero at all levels,
2. have a constant nonzero wind speed in height, i.e., no wind shear, and
3. zero at the inversion height with a constant nonzero wind shear.

For the "no initial wind" simulations (Figure 4), the results using $N_{aco} = 6$ and 12 are in close agreement and have, thus, converged. For the "no wind shear" simulations, the difference between the two N_{aco} simulations is even slightly larger than in the control set of simulations indicating non-convergence. Lastly, for the "zero wind speed at inversion" simulations, the $N_{aco} = 6$ and 12 simulations are in close agreement, showing convergence. Therefore, we conclude that large wind speed at the inversion height is a contributing factor to the lack of convergence in the DRF02 case. The degree of sensitivity to varying wind speed is further analyzed in Section 2.2. Interestingly, although wind shear is generally considered to be an important factor for cloud-top entrainment that contributes to cloud dissipation, shear is not a control factor for the convergence issue.

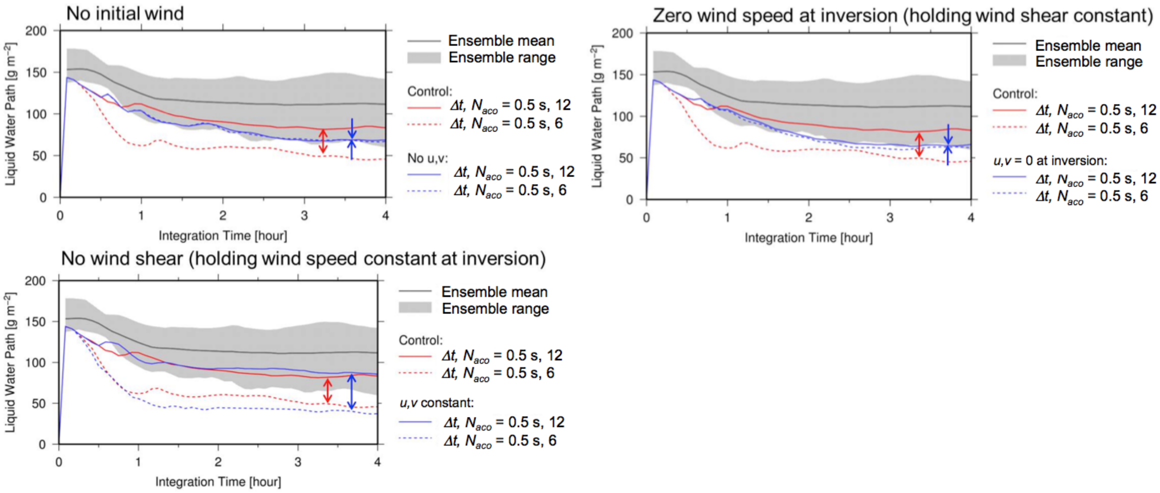

Figure 4. As in Figure 1 but with the sensitivity tests of the initial wind profile, as described in the text. Large differences between the solid and dashed blue lines indicate the presence of the convergence issue. Note the sensitivity simulations converge to a different solution than the control simulation (solid red line) because of the change in initial wind profiles. Colored arrows indicate directly comparable simulations.

The sensitivity of LWP over time to changes in the magnitude of the moisture jump at the inversion height as shown in Figure 5. The DRF02 case uses a simple step function of total water to define the moisture jump at the inversion that can be written as $\Delta q_{\mathrm{v}} = (q_{bot} - q_{top})$, where q_{top} is the water vapor at the top of the inversion (= 5 g kg^{-1}) and q_{bot} is the water vapor at the bottom of the inversion (= 8.6 g kg^{-1}), and Δq_{v} is the water vapor difference (moisture jump) across the inversion (= -3.6 g kg^{-1}). For DRF02, the absolute value of the moisture jumps in the sensitivity tests, reduced from the control by 1 and 2 g kg^{-1} (using $q_{top} = 6$ and 7 g kg^{-1}, respectively). From Figure 5, changes to N_{aco} in simulations with a 1 g kg^{-1} smaller moisture jump yield smaller differences in LWP than for the control simulations, meaning that acoustic sub-step dependency is reduced with a smaller moisture jump. The simulations converge when a 2 g kg^{-1} smaller moisture jump is used, with the acoustic sub-step dependency being totally removed. The sensitivity tests using even smaller moisture jumps also converge for different N_{aco} (not shown). The degree of the sensitivity of convergence to the magnitude of the moisture jump is further analyzed in combination with horizontal wind speed in Section 2.2.

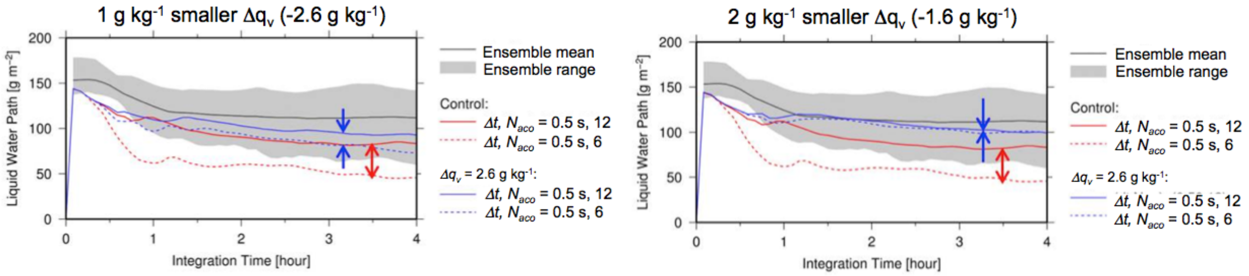

Figure 5. As in Figure 1, but for sensitivity tests that reduce the moisture jump at the inversion.

While Figures 4 and 5 demonstrate the primary factors leading to non-convergence are wind speed and moisture gradient both at the inversion height, the figures do not indicate why. To better understand the processes leading to non-convergence, one needs to examine the model results when the non-converged and converged simulations start to diverge. Therefore, Figure 6 shows vertical cross sections of horizontal wind components, potential temperature perturbation, water vapor perturbation, and water vapor tendency due to condensation/evaporation 30 minutes into the simulation period for the control simulations. The non-converged N_{aco} = 6 simulation has small-scale fluctuations in the horizontal winds that do not appear in the converged N_{aco} = 12 simulation. These wind fluctuations are collocated with the fluctuations in potential temperature, water vapor, and condensation/evaporation. The wind fluctuations are not found in the converged sensitivity simulations using smaller wind speed or moisture jump at the inversion. Similar non-converged results are obtained from the "wind only" simulation in which all forcings and physics packages are turned off except for the microphysics. Thus, the wind fluctuations associated with large wind speed and moisture jump could be responsible for the non-converged results. As described later, similar wind fluctuations are found before the cloud formation in an ARM SGP case and the cloud-top evaporation and condensation seem to enhance the spurious wind fluctuations.

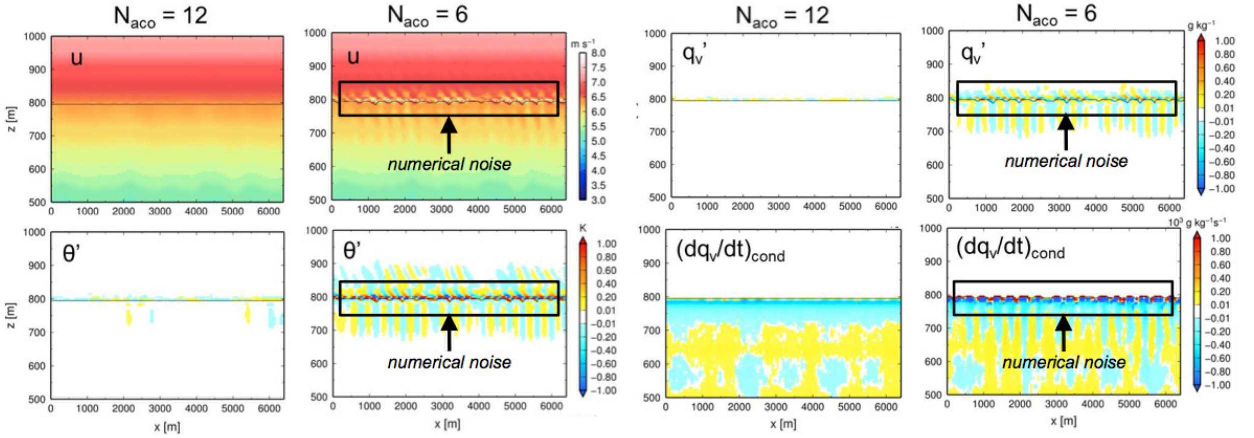

Figure 6. Vertical cross section of the east-west component of horizontal wind, u (m s^{-1}), potential temperature perturbation, *θ*' (K), water vapor perturbation, q_v' (g kg^{-1}), and water vapor tendency due to evaporation and condensation, $(dqv/dt)_{cond}$ (g kg^{-1} s^{-1}), 30 minutes into the DRF02 simulation period using N_{aco} = 6 and 12.

SGP cases: In parallel with the DRF02 simulations, over one hundred LES sensitivity simulations have also been performed for shallow cloud cases at the SGP site. These were conducted to understand how the numerical issue impacts realistic conditions pertinent to ARM over land. Two representative cases are discussed in this section. The results are analyzed similarly to the DRF02 case and predicted cloud amounts are compared with available measurements. We confirm the same acoustic time-step dependency issue occurs when strong inversions exist at the boundary-layer top for the realistic shallow cloud conditions over land.

The morning sounding on 13 May 2008 at the SGP site, shown in Figure 7, is an example of an extreme case in terms of the moisture jump at the boundary-layer top, based on the climatological analysis presented in Section 2.3. A strong gradient exists for all four variables between the boundary layer (up to ~1.2 km) and the free troposphere. The jump in specific humidity is extremely large, decreasing from ~13 g kg^{-1} to 1 g kg^{-1} in the free atmosphere. As will be seen later, for non-converged model configurations, the numerical noise first appears at the inversion height shortly after the simulation start time, consistent with the behavior in the idealized DRF02 case, but starts before the formation of cloud. This suggests that the numerical noise is not caused by feedbacks associated with cloud microphysics parameterizations but, instead, points to the noise likely being due to a fundamental deficiency in the dynamical core, which is pursued in Section 2.4.

Figure 8 shows another test case where no sharp vertical gradient is present in the initial profiles for 14 May 2007. On this day, the specific humidity gradually decreased from 13 g kg^{-1} near the surface to ~3 g kg^{-1} at about 3.8 km. This day is more representative of the meteorological conditions observed at the SGP site as will be shown in Section 2.3. No time-step sensitivity is found with WRF for this case.

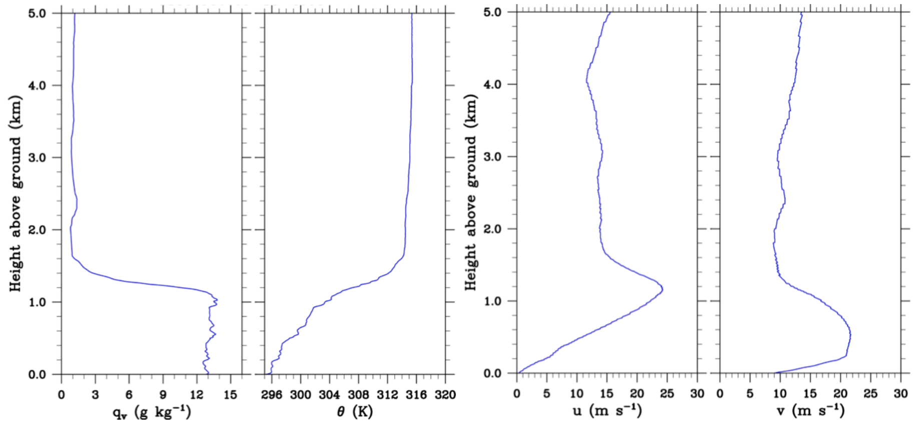

Figure 7. Profiles of water vapor mixing ratio, potential temperature, and winds for 13 May 2008 at 11:30 UTC, a case where WRF's behavior resembles the convergence issue of DRF02.

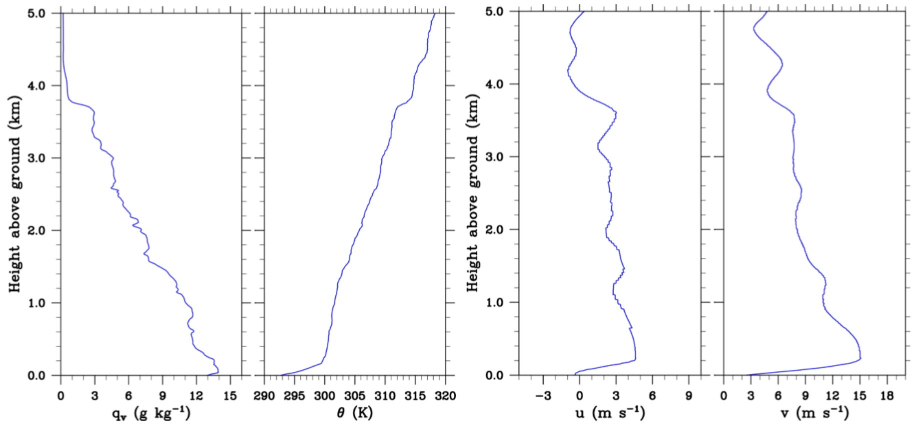

Figure 8. As in Figure 7, but for 14 May 2007 at 11:30 UTC, which is a more "typical" case for the SGP site where WRF does not exhibit the convergence issue.

Three simulations are presented here were performed for each case to demonstrate how time-step settings impact cloud evolution. All the simulations reported here are 15-h long (starting from 06:00 LST, using the initial profiles from Figures 7 and 8) with prescribed surface fluxes from ARM observations and a grid spacing of 100 m. The left panels in Figure 9 show the evolution of total cloud fraction and LWP for the 13 May 2008 stratocumulus case for different time-stepping choices. The right panels show the corresponding results for the 14 May 2007 cumulus case. It is clear the convergence issue only exists for the 13 May 2008 case that has the strong inversion. For the simulation using $\Delta t = 0.5$ s and $N_{aco} = 6$ (red line), the peak LWP is 62 g m^{-2}, which is much lower than the peak value of 97 g m^{-2} when using 12 acoustic sub-steps (black line). For the 17 May 2007 case, there is no appreciable sensitivity in either LWP or total cloud fraction to the number of acoustic sub-steps for the given time-step choice. Note that there are some differences between the observed and simulated clouds, which are partly due to not forcing the simulations with time-varying large-scale tendencies. This can lead to issues such as preventing the simulations from generating the afternoon peak in LWP for the 13 May 2008 case. The choice of surface flux forcing data sets also noticeably impacts the results (not shown). However, we have decided not to complicate the simulation setup with changes to the surface flux treatment because the objective of these simulations is to examine the impact of the time-stepping dependency, and a qualitative reproduction of the clouds is sufficient for this purpose.

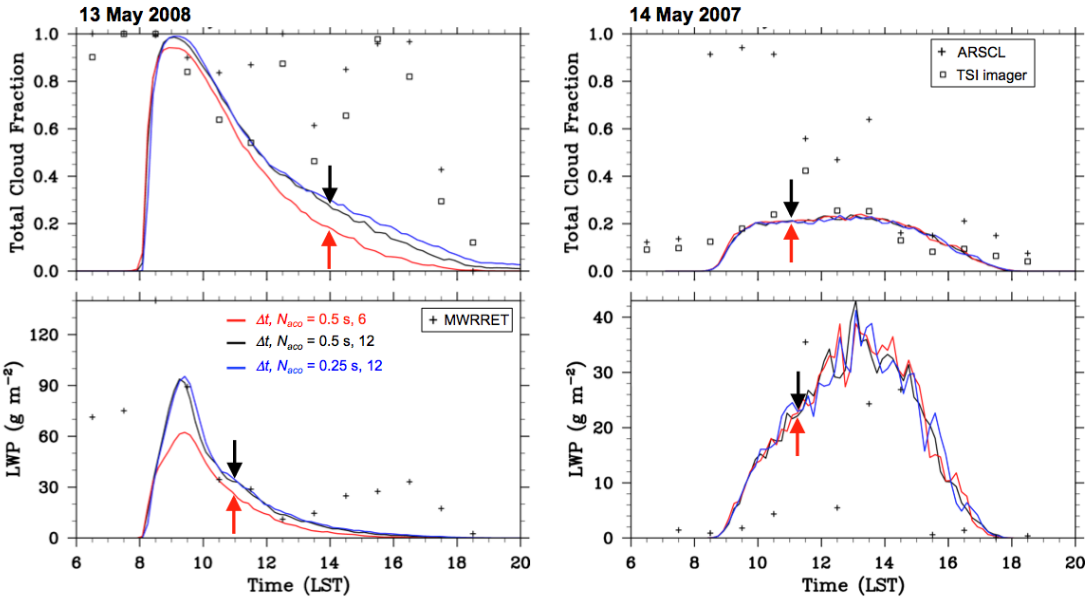

Figure 9. Total cloud fraction and LWP evolution for the 13 May 2008 (left) and 14 May 2007 (right) cases at the SGP site. Red lines denotes $\Delta t = 0.5\ s$ with 6 acoustic sub-steps ($N_{aco} = 6$), black lines denotes $\Delta t = 0.5\ s$ time step with 12 acoustic sub-steps ($N_{aco} = 12$), and blue lines denote $\Delta t = 0.25\ s$ with 12 acoustic sub-steps ($N_{aco} = 12$). The squares and crosses in the upper panels are total cloud fraction from the total-sky imager (TSI) and the ARSCL data product, respectively, while the crosses in the lower panel are LWP from the microwave radiometer (MWRRET). Arrows indicate the sensitivity to N_{aco} for the non-converged configuration.

We also performed sensitivity experiments with the 13 May 2008 case where we artificially changed the jump in specific humidity or wind speed near the inversion height. Consistent with the results from DRF02, the SGP case exhibits numerical noise near the inversion that is very sensitive to the magnitude of the moisture jump, and when we reduce the wind speeds to near zero the noise disappears (not shown).

Figure 10 shows the numerical noise for the 13 May 2008 case first appears at the inversion height shortly after the simulation start time, consistent with the behavior in the idealized DRF02 case. For the 13 May 2008 case, when using $\Delta t = 0.5$ s and $N_{aco} = 6$, WRF produces numerical noise in vertical velocity, temperature, and moisture near the inversion only 30 minutes into the simulation and before the formation of clouds. The signal near the inversion (~1.2 km) is so big that the initial random perturbations imposed near the surface to induce turbulence as the model spins up are swamped and not even visible for the color scale that clearly delineates the numerical noise. However, unlike for DRF02 where conditions induce cloud formation immediately at the model start time, the SGP case is cloud-free for the first several hours, and the noise starts before clouds form. This demonstrates the numerical noise is not caused by feedbacks between advection/diffusion errors and the cloud microphysics parameterizations. Later, when clouds form, there also appears to be erroneous interactions between the vertical velocity and cloud-top evaporation/condensation, which seem to enhance the spurious wind fluctuations. However, these cloud interactions are a symptom of the problem and not the root cause.

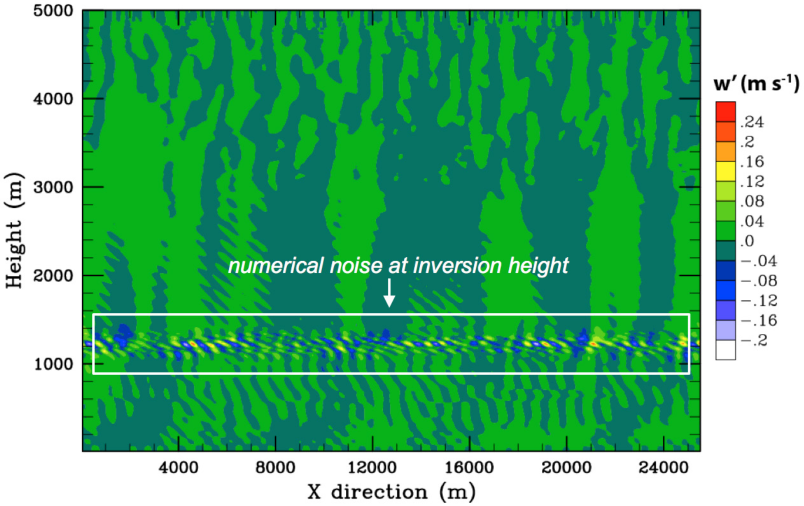

Figure 10. A vertical cross section of perturbation vertical velocity (m s^{-1}) 30 minutes after the model initialization when Δt = 0.5 s and N_{aco} =6 for the 13 May 2008 case. This simulation corresponds to the red line in the left panels of Figure 9. The simulation at this time is for clear-skies, as clouds do not form for another 1.5 h.

Combining the results from the DRF02 and SGP simulations gives a clear picture of the conditions conducive to the convergence issue and suggests the source of the problem, if not the specific cause. Our hypothesis is that when too long of a dynamics time step is used, combined with too few acoustic sub-steps for a given dynamics time step, WRF becomes susceptible to numerical noise in the presence of large vertical moisture gradients combined with non-negligible wind speeds. This noise then impacts subsequent cloud formation through slightly earlier cloud formation and increased mixing between the boundary layer and free troposphere that ultimately leads to fewer shallow clouds forming during the day.

In both the DRF02 and SGP cases, the numerical noise can be made smaller by shortening the dynamics time step or increasing the number of acoustic sub-steps (not shown). Small numerical noise is still present when shortening the time step to 0.25 s with 12 acoustic sub-steps. However, this reduces the noise by an order of magnitude, and it no longer impacts the cloud characteristics, which is why convergence is reached for a sufficiently small time step and large number of acoustic sub-steps. The convergence issue itself arises from the large vertical velocities that form through the numerical noise, which in turn generate localized regions of artificially enhanced supersaturation where clouds form prematurely. The noise also leads to additional mixing between the boundary layer and free troposphere. The net effect is reduced clouds throughout the day and an overall poor simulation. It should be noted that the numerical noise is unlike traditional numerical errors that grow exponentially until the model crashes, such as those produced through violation of the Courant-Friedrichs-Lewy (CFL) condition. In the present case, the numerical noise exhibits an initial growth period and then stabilizes without further growth. Thus, the model does not crash, yet it produces an erroneous solution.

2.2 Methods to Detect Noise and Convergence Issues

Based on the above sensitivity tests, we developed a methodology to detect the numerical noise that leads to the convergence issue. This permits users to detect the problem within the first hour, and adjust their simulations without having to generate a complete set of simulations to determine whether they are affected. The method also allows us to quantitatively demonstrate how various combinations of moisture jumps and wind speeds impact noise generation.

The noise is easily detected early in a simulation before cloud features emerge, as seen in Figures 6 and 10 and further shown in Figure 11. The telltale signature for the noise is its small-scale structure, on the order of the model's effective resolution, and presence near regions with strong vertical moisture gradients. By applying a Fourier transform to the wind fields from our LES simulations, we find most of the signal from fluctuations causing non-convergence has a spatial scale smaller than 400–500 m for the DRF02 case. Based on this, the signal can be isolated from the background field by employing a high-pass filter on the wind field. For example, a high-pass filter applied to the perturbation zonal wind field, $u' = u - u_{mean}$, or wavelengths $\lambda < 400$–500 m has been found effective for detecting the initiation of the instability in the DRF02 case, prior to the growth of the turbulent boundary layer. We then quantify the magnitude of the noise through the variance of u after it has been high-pass filtered to remove wavelengths longer than 400 m.

Figure 11 compares vertical profiles of u variances and cloud fractions from DRF02 before and after filtering out wavelengths longer than 400 m using an inverse Fourier transformation. At 15 min into the integration time, there is a distinct peak in the unfiltered wind fluctuations near the inversion in the non-converged simulation ($N_{aco} = 6$), which also remains after filtering. At 30 min, there is no clear difference between the converged and non-converged simulations before the filtering because of similar u variance peaks arising from developed boundary-layer turbulence. However, the signal from the spurious u fluctuations becomes evident after filtering out wavelengths longer than 400 m.

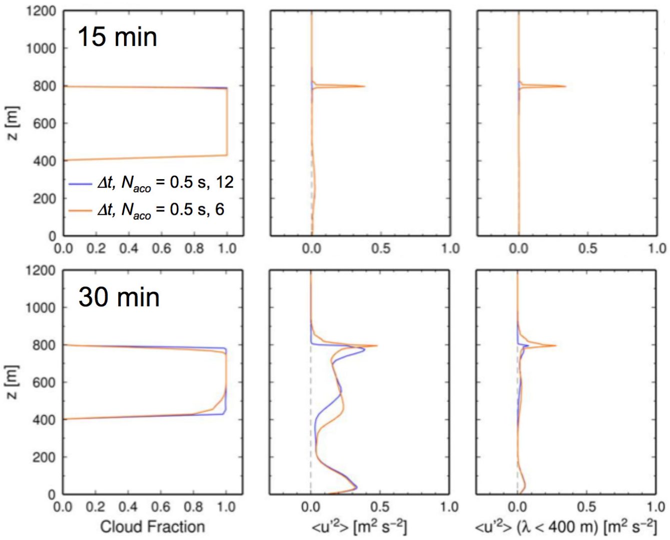

Figure 11. Vertical profiles of cloud fraction, and unfiltered and filtered u variances at 15 and 30 min into the integration period for the DRF02 case, using $N_{aco} = 6$ and 12. The filtering removes wavelengths longer than 400 m.

To demonstrate the maximum value of u variance in the vertical profile can be a measure of the spurious fluctuations, we present the maximum u variance in the simulations initialized using different constant wind speeds. As illustrated in Figure 12, the unfiltered maximum u variances (dashed lines) for simulations using $N_{aco} = 12$ and 6 exhibit different time variations and similar relative magnitudes for different initial wind speeds, making it difficult to detect differences between converged and non-converged simulations. By applying the filter (solid lines), the spurious *u* fluctuations are negligible for $N_{aco} = 12$ but are clear for $N_{aco} = 6$.

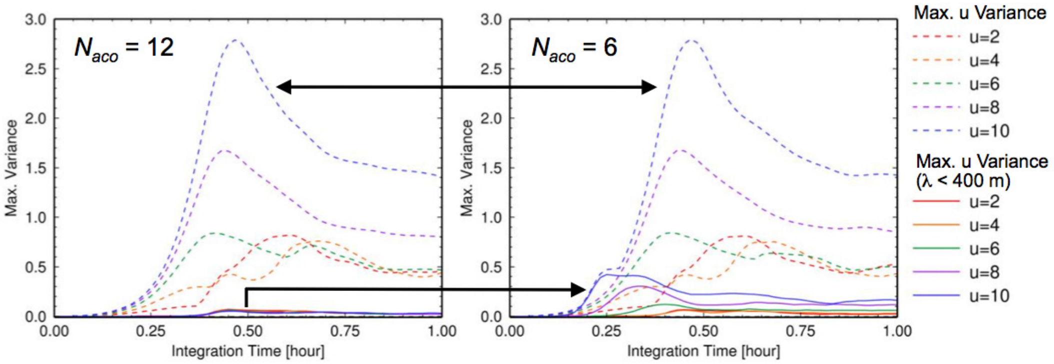

Figure 12. Unfiltered (dashed lines) and filtered (solid lines) maximum *u* variances for the DRF02 case from simulations using $N_{aco} = 6$ and 12 and different initial wind speeds that are constant with height. Results are shown for $u = 2$, 4, 6, 8, and 10 m s^{-1} with $v = 0$ m s^{-1}.

Finally, using the maximum filtered-wind variance as a measure of the spurious wind fluctuations, the acoustic sub-step dependency is examined in a 2D parameter space of wind speed and moisture jump at the inversion height for DRF02 using 3D simulations. Figure 13 shows maximum *u* variance averaged over the first 30 min of the integration as a function of wind speed and moisture jump Δq_v. Before applying the filter (top panels), the *u* variance increases strongly with wind speed, leading to a striped pattern that hides the signal from the spurious *u* fluctuations. By applying the filter (bottom panels), the signal from the spurious wind fluctuations is evident and shows that maximum variances increase for larger wind speeds and larger moisture jumps (more negative Δq_v). The new metric can be used for automatic detection of the spurious wind fluctuations causing the convergence issue, and might also be useful to detect other potentially problematic numerical noise in operational simulations.

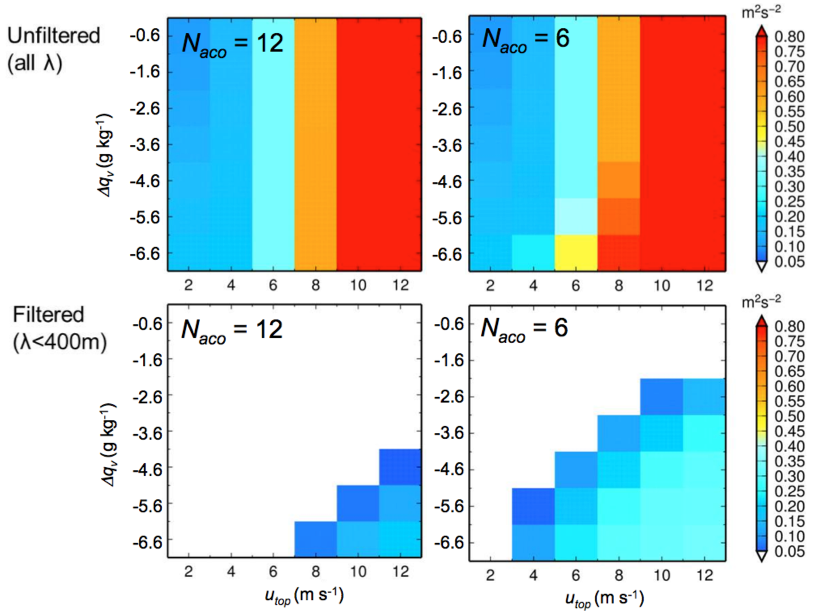

Figure 13. Unfiltered and filtered maximum u variances (color) as a function of initial wind speed at the inversion top (u_{top}) and the moisture jump at the inversion, $\Delta q_v = q_{bot} - q_{top}$. The DRF02 control simulation values at initiation are $u_{top} = 6.4$ m s^{-1}, $\Delta q_v = 3.6$ g kg^{-1}. The control case also has $v_{top} = 4.5$ m s^{-1}, which is not considered here (i.e., the response of the advection scheme to wind uses only one component).

2.3 Climatological Study of Conditions Conducive to Convergence at the SGP Site

Since the analyses performed for the DRF02 and SGP cases show that the numerical noise is generated when there are large moisture differences across the inversion in the presence of sufficiently large wind speeds, we have used the ARM Planetary Boundary Layer (PBL) Value-Added Product (VAP) (Sivaraman et al. 2013) between 2001 and 2013 to quantify how frequently these boundary-layer conditions occur at the SGP site.

Radiosonde measurements are one of the most common data sources used to determine PBL height and inversion depth. The definition of the PBL height is somewhat subjective and has often been determined manually by analyzing vertical profiles of potential temperature and moisture. Alternatively, several methods have been proposed (Seibert et al. 2000) to automatically estimate the PBL height. Differences among the methods can be considered a partial quantification of the uncertainty in the PBL height. The ARM PBL VAP uses the Heffter (1980), Liu and Liang (2010), and the bulk Richardson number (Sorenson et al. 1998) methods to estimate PBL height, and differences between the three methods can be considered a partial quantification of the uncertainty in the PBL height. These methods are applied to all the available radiosondes launched at the SGP site between 2001 and 2013. Radiosondes at the SGP site are usually launched four times per day (around 00, 06, 12, and 18 UTC), but during intensive observation periods there may be as many as nine radiosondes launched per day. Over the 13-year period in the PBL VAP, there are data from 17,979 radiosondes.

In our analysis, we use the estimates from the Heffter (1980) method, but only when the three methods are within 15% of one another. This is a rather stringent criterion. There are 10,030 radiosondes that both met this criterion and remain for analysis, or ~56% of the total number of radiosondes. The annual number of radiosondes that met this criterion ranged from 483 (2013) to 849 (2002). While this removes 44% of available data, there are still a substantial number of radiosondes available to derive a climatology of boundary-layer characteristics over the SGP site. In addition to PBL height, we also use the potential temperature, specific humidity, and wind speeds at the top and bottom of the inversion depth to compute the vertical differences and gradients of those quantities. In addition to the overall frequency of occurrence, yearly and seasonal statistics were computed.

Figure 14 depicts the seasonal variations of the potential temperature gradient across the inversion depth at the top of the boundary layer over the SGP site. Most values are between 0.02 and 0.3 K m^{-1}, and the number of occurrences drops significantly for higher potential temperature gradients. The overall statistics do not change significantly from season to season. However, there is a minimum during the summer, with a mean value of 6 per year, for potential temperature gradients greater than 0.04 K m^{-1}.

The seasonal variability of the specific humidity across the inversion depth over the SGP site is shown in Figure 15. The specific humidity difference associated with the 13 May 2012 LES simulation described in Section 2.1 was between −12 and −10 g kg^{-1}. The total number of occurrences between 2001 and 2013 equal to and greater than this difference was 21 (0.9% of the time) and 18 (0.8% of the time) during the spring and summer, respectively. Therefore, very large differences in specific humidity across the inversion do not happen frequently. But wind speed at the inversion height is another factor. Based on the 2D sensitivity analysis of convergence in Figure 13, moisture jumps larger than 2 g kg^{-1} across the inversion is potentially problematic for wind speeds ~12 m s^{-1}. Extending those findings to a joint distribution derived from the PBL VAP shown in Figure 15 indicates potentially problematic conditions occur for ~8% of the radiosondes between 2001 and 2013 (ranging from 5.6% in 2006 to 10.9% in 2011), with the greatest frequencies occurring in spring and summer.

However, the following will show two methods that can minimize the impact of the noise in the default version of WRF. Further, by altering its dynamical core, the issue can be eliminated entirely.

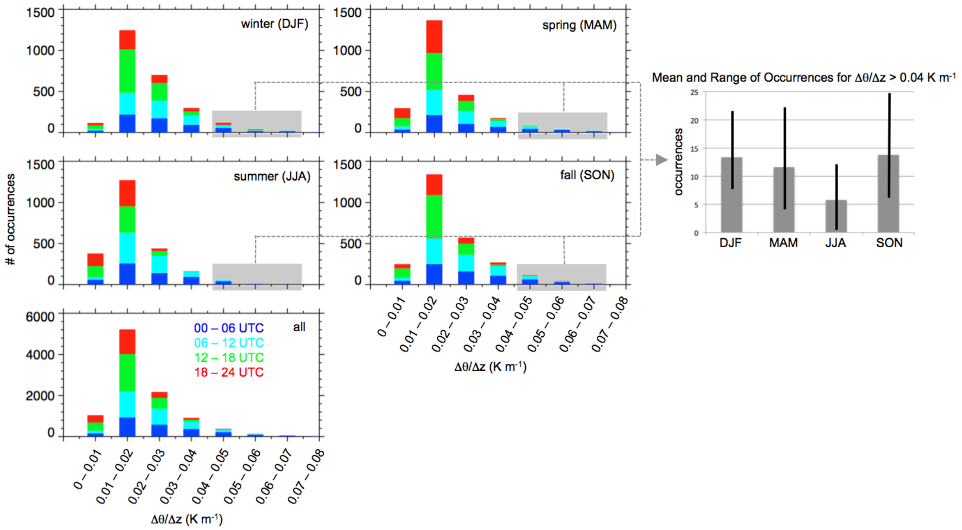

Figure 14. Climatology of potential temperature gradient across the inversion depth at the top of the boundary layer over the SGP site between 2001 and 2013.

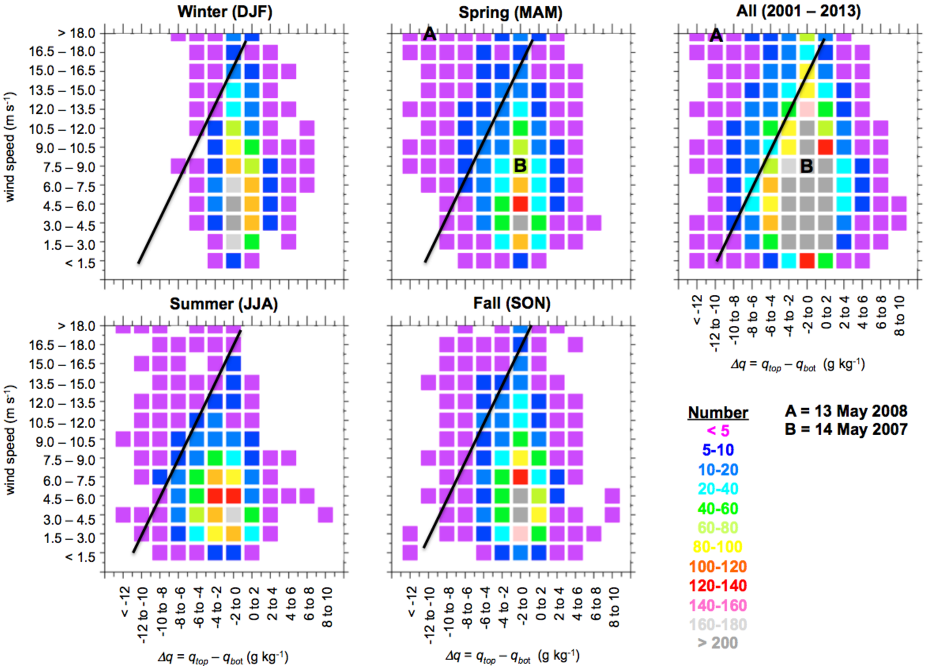

Figure 15. Joint frequency distribution of specific humidity difference and average wind speed over the inversion depth at the SGP site between 2001 and 2013. A and B (in the Spring and All panels) denote the radiosondes shown in Figures 7 and 8. The line corresponds to values where time-step convergence was an issue from the DRF02 sensitivity study shown in the lower left panel in Figure 13. Conditions left of the line are predisposed to exhibiting the convergence issue, and to the right of the line, the issue is not likely to impact results.

2.4 Ways of Eliminating the Convergence Issue

Our team has identified three methods that can be applied to address the convergence issue in WRF. Each has its advantages and disadvantages.

Galilean transformation: A technique sometimes used with LES modeling to permit longer time steps is to apply a Galilean transformation to the domain (e.g., Matheou et al. 2011; Wang et al. 2010). We implemented this capability in WRF to reduce the effective wind speed at the inversion height, which subsequently inhibits the generation of spurious fluctuations by the advection scheme. Mathematically, a Galilean transformation is used to transform between the coordinates of two reference frames that differ only by a constant relative motion. Since the Newtonian equations of motion are invariant under a Galilean transformation, the transformation is applicable to LES to simulate motion on the moving coordinate ($\boldsymbol{v}^*$) instead of on the static coordinate ($\boldsymbol{v}$), which differ by a constant relative velocity $\boldsymbol{V}_c$: $\boldsymbol{v} = \boldsymbol{v}^* + \boldsymbol{V}_c$. The net effect of this transformation is a reduced wind speed ($\boldsymbol{v}^* = v - V_c$) that permits using a longer time step under the CFL limit, increasing computational efficiency. Theoretically, results are identical between simulations with and without the transformation. In practice, small differences may arise from minor time-step dependencies in the parameterizations and advection algorithms.

In our implementation, prognostic horizontal wind components are transformed to a moving coordinate using $\boldsymbol{V}_c$ at the beginning of the time step, and the horizontal wind components are recovered to the original frame of reference at the end of time step to accumulate statistics for output. The untransformed horizontal wind components are used for the Coriolis force, interactions with the surface (momentum and heat fluxes), the other physics parameterizations, and model-top damping. We also developed a function that updates $\boldsymbol{V}_c$ over the integration time, based on a sampling of the simulated domain-averaged winds at an arbitrary height for a given time period. In the implementation, $\boldsymbol{V}_c$ is constant for each time period (or time step) so there is no acceleration of the coordinate.

Figure 16 shows the 12-h time evolution of cloud properties in DRF02 simulations using Galilean transformations with fixed and temporally varying $\boldsymbol{V}_c$. The fixed $\boldsymbol{V}_c$ simulations set $\boldsymbol{V}_c$ to the horizontal wind speed at the inversion height in the initial profile. The varying $\boldsymbol{V}_c$ simulations update $\boldsymbol{V}_c$ by sampling winds at 800 m height in 10 min intervals. The fixed $\boldsymbol{V}_c$ simulations (blue lines) yield good agreement with the control simulations (red lines) for the first 4 h of the simulation; however, after 4 h, cloud fraction in the simulation using $N_{aco} = 6$ begins to depart from the converged control simulation and becomes markedly different by 8 h. Using a time-varying $\boldsymbol{V}_c$ (green lines) does not have this problem and yields convergence for the whole period. The convergence obtained by using a time-varying $\boldsymbol{V}_c$ is attributed to the flexibility in maintaining $\boldsymbol{V}_c$ close to the wind speed at the inversion that, as shown in Figure 17, varies considerably during the simulation period and cannot be adequately represented by a fixed value.

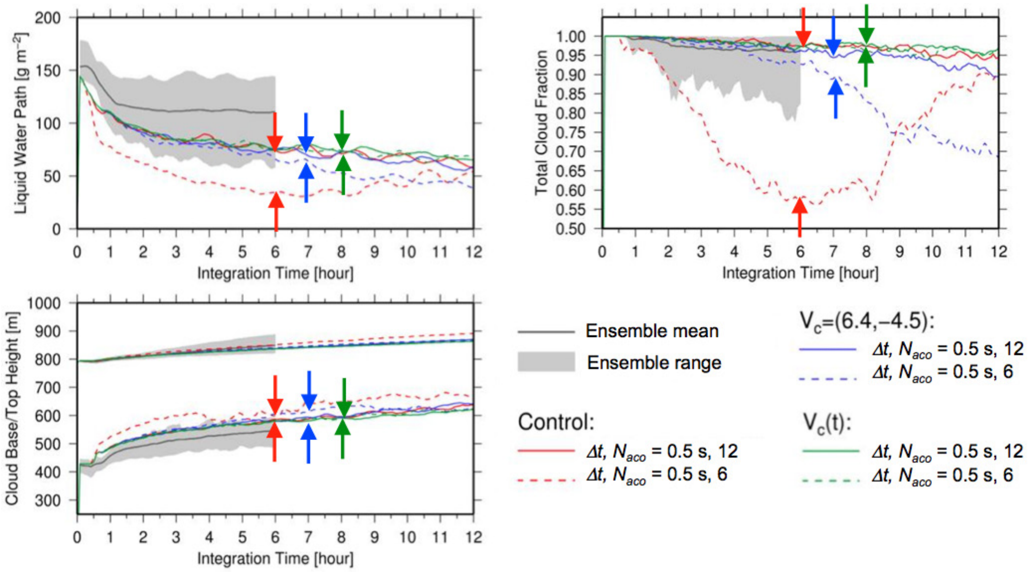

Figure 16. As in Figure 1, except for simulations using Galilean transformations with a fixed V_c (blue) and temporally varying V_c (green).

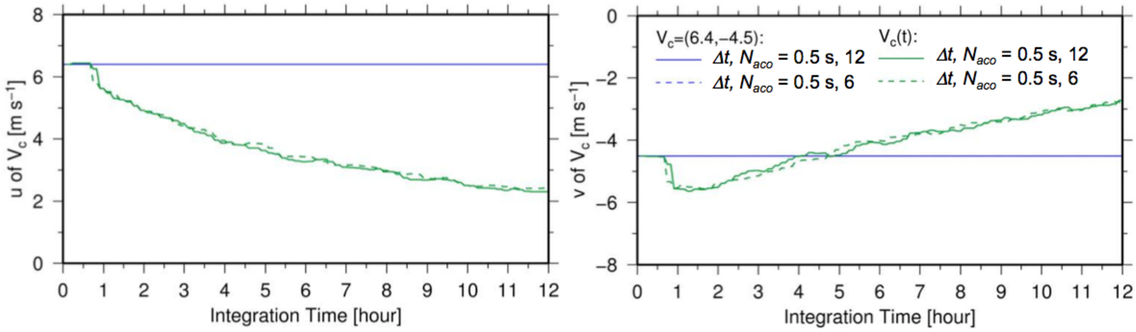

Figure 17. Time series of the wind components of the fixed V_c (blue) and time-varying V_c (green).

Application of our high-pass filter metric confirms the simulations using a Galilean transformation do not generate the spurious wind fluctuations, and we also verified that vertical profiles agree closely with a converged reference simulation (not shown).

As mentioned above, this transform methodology is most appropriate for doubly periodic domains. Non-periodic domains where the wind is not initialized, and forced uniformly, will need complicated treatments of prognostic variables at the boundaries. As a solution for the convergence issue, the methodology relies on the wind speed being relatively uniform at the level of the moisture jump. For LES domains where this may not be true, the numerical noise could erupt sporadically throughout the domain where the transformed wind speed is greatest. The methodology can reduce the computational cost since it enables one to use a larger time step. However, it is not a perfect solution for the convergence issue as it is not completely robust across all conditions.

WENO advection: Our team contacted Branko Kosovic (NCAR), another experienced LES modeler, for his opinion on how to deal with the numerical issues in WRF. He had not observed these issues in WRF, but suggested testing the Weighed Essentially Non-Oscillatory (WENO) advection scheme (Liu et al.,

1994) that was implemented in WRF version 3.4. WENO is based on the Essentially Non-Oscillatory (ENO) advection scheme, which is an improved up-wind difference scheme that uses a constraint function to prevent overshooting and undershooting the solution. ENO prepares three constraint functions based on higher-order derivatives, and selectively use the smoothest function. WENO uses a weighted average of all three functions to prevent overshooting or undershooting of the solutions and inhibit the generation of numerical noise due to the finite-difference approximations. To examine the impact of WENO, our team ported the LES packages from YF12 to WRF v3.6.1, the most recent version available at the time of this report. We find that replacing the default momentum advection scheme and the monotonic scalar advection scheme with the WENO advection scheme for momentum and scalars significantly reduces the numerical noise in the DRF02 and SGP cases.

Figure 18 shows the time variation of cloud properties in the DRF02 case with and without using the WENO scheme. The simulations using WENO converge for the two different N_{aco} values shown (6 and 12). The predicted cloud decks are slightly more solid in the WENO simulations than in the control simulations, having slightly greater LWP and cloud fraction, but the WENO simulations are within the ensemble range of the other LES models (gray shading). Our high-pass filter metric shows substantially improved behavior for the spurious *u* fluctuations when using WENO, with the generation of *u* fluctuations inhibited by WENO (not shown).

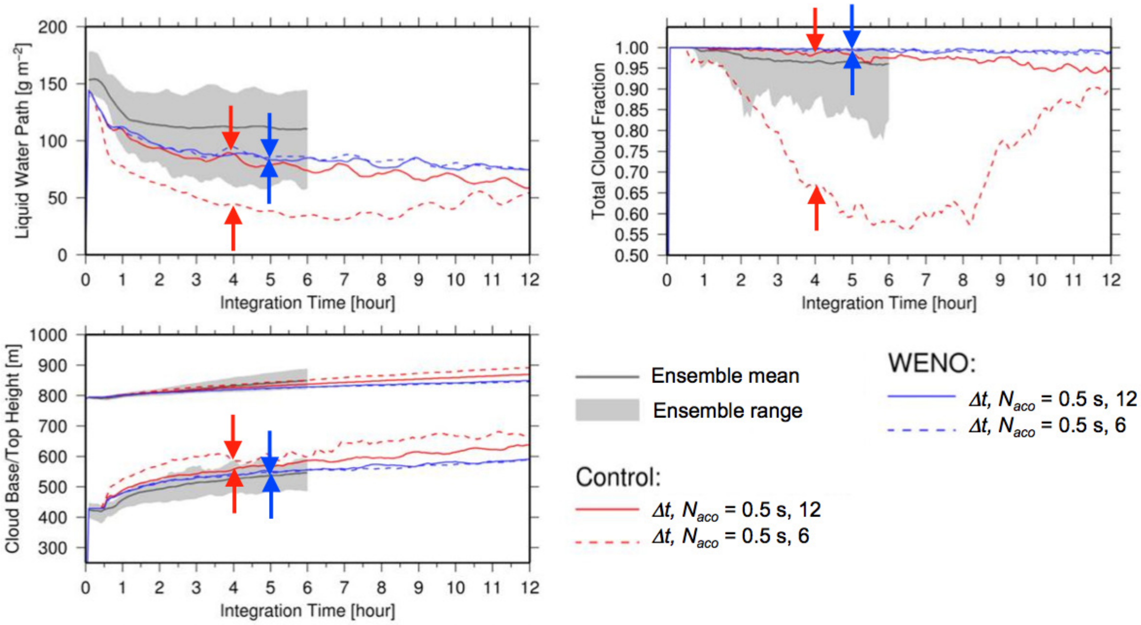

Figure 18. As in Figure 2, except for the sensitivity test using the WENO advection scheme for the DRF02 case.

The improvement with WENO for the SGP case is shown in Figure 19, as seen by comparing Figures 19 and 10 (both use the same color scale). Increasing the divergence damping (*smdiv* in the WRF "namelist" input file) from the default value of 0.1 to 0.3 also helps WENO produce better convergence when changing the time stepping. This noise reduction is commensurate with a significant decrease in the sensitivity of LWP and total cloud fraction to time-stepping choices. As shown in Figure 20, there is a large change in LWP when changing the number of acoustic sub-steps from 12 to 6 with the default advection scheme (dashed lines). The WENO advection scheme almost completely removes the sensitivity (solid lines).

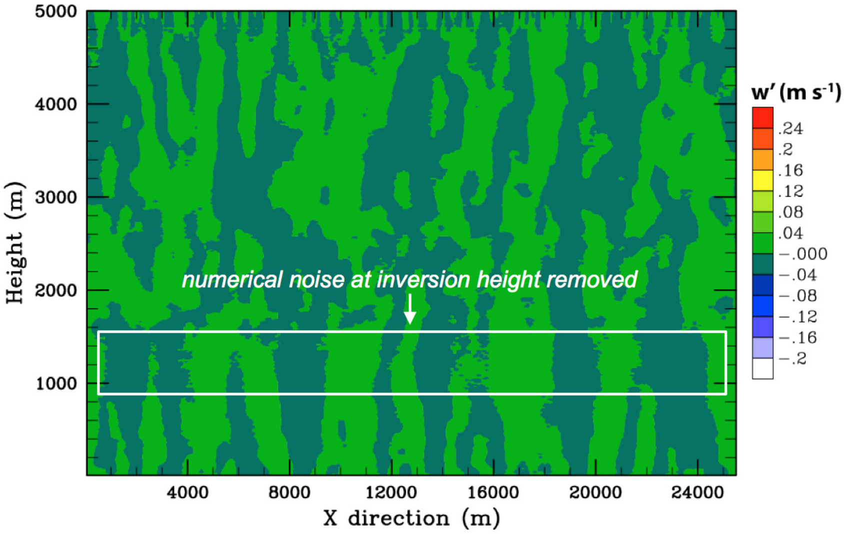

Figure 19. As in Figure 10 for the 13 May 2008 SGP case, except the WENO advection scheme is used for momentum and scalars. The high-frequency variability seen in Figure 10 is removed.

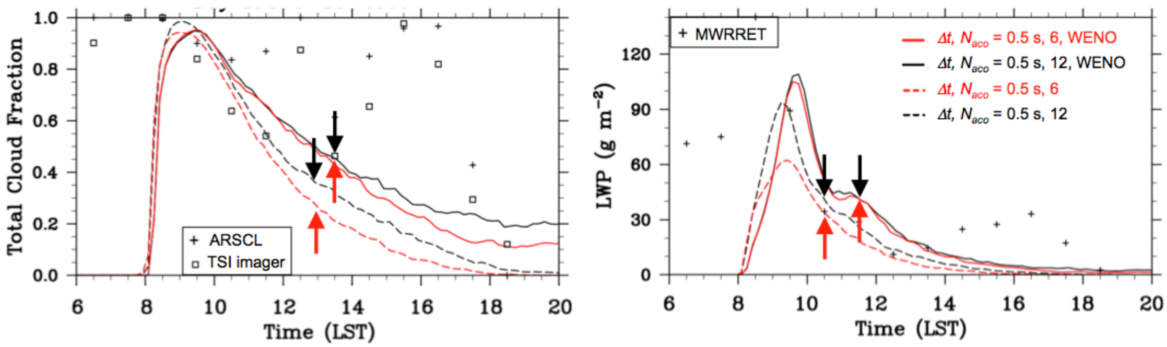

Figure 20. Total cloud fraction and LWP evolution for the 13 May 2008 case with Δt =0.5 s where the red lines denote N_{aco} = 6 and black lines denote N_{aco} = 12. Dashed lines are for the default momentum advection scheme combined with monotonic scalar advection, and solid lines are for the WENO momentum and scale advection schemes. Arrows depict the sensitivity to N_{aco} for the different advection configurations.

While the use of the WENO advection scheme seems to eliminate the numerical noise and convergence time-step sensitivity, it is unclear whether the numerical method is superior to other advection options in WRF or whether application of WENO is merely suppressing the numerical noise that forms. We conclude that the WENO scheme mitigates the production of the spurious wind fluctuations and can yield convergence.

Modifications to the dynamical core: Determining the best approach for handling the convergence time-step sensitivity depends on the source of the problem. To better isolate the source, we conducted additional tests using an early 2D WRF prototype model that uses a height-coordinate-based formulation of the equations, instead of the mass-coordinate-based equations as in the modern versions of WRF. The height-coordinate-based version considers moisture when calculating pressure perturbations within the acoustic sub-steps, while the mass-coordinate-based version does not, which we had suspected to be the cause of the numerical noise. Simulations from both model versions using the 13 May 2008 SGP case with the physics parameterizations turned off, i.e., the test is purely of the dynamical core, reveal that the height-coordinate-based WRF does not exhibit the numerical noise while the simplified configuration with the mass-coordinate-based version acts like the full 3D cases (not shown).

With this information, we contacted Bill Skamarock and Joe Klemp (NCAR), the original developers of the WRF dynamical core. They reproduced the problem and proposed replacing potential temperature with moisture-weighted potential temperature in the WRF dynamical core. This solution treats the pressure perturbation consistently for both the regular dynamic time step and the acoustic sub-steps by taking into account contributions from moisture perturbations throughout the equation system. This involves changing only a few lines of code in solve_em.F, one of the primary WRF subroutines. Our subsequent tests with this solution confirm that this modification does indeed remove the numerical noise.

As shown in Figure 21, we can see clearly that with the modified dynamical core the numerical noise in the perturbation vertical velocity near the inversion is completely gone for the 13 May 2008 SGP case. It is important to note that without the modification the numerical noise persisted 120 minutes, just before the initiation of clouds, and contributed to the earlier cloud initiation in that simulation.

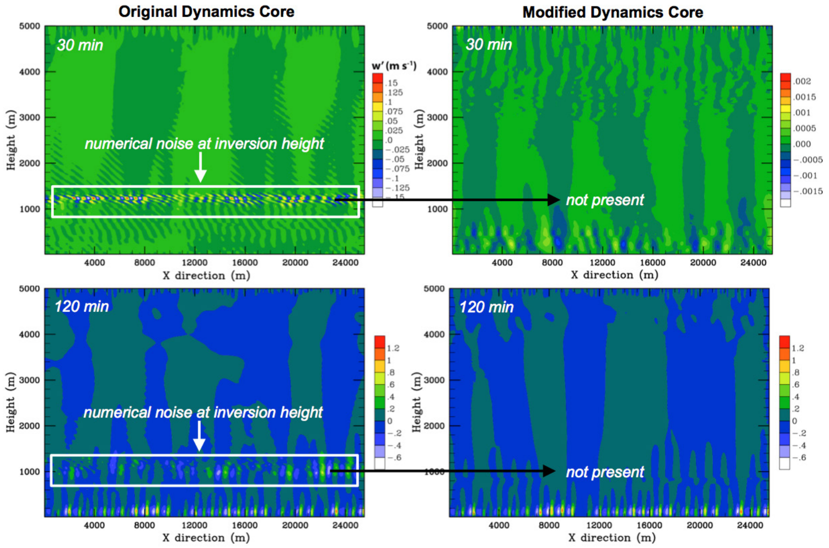

Figure 21. Vertical cross sections of the perturbation vertical velocity field (m s^{-1}) from two WRF-LES simulations for the 13 May 2008 case with $\Delta t = 0.5\ s$ and $N_{aco} = 12$, (left) without the modification, and (right) with the modification. The upper panels are snapshots 30 minutes into the simulation, and the lower panels are120 minutes into the simulation.

With the modified dynamical core, the convergence problem in terms of LWP and total cloud fraction is also resolved, as shown in Figure 22. With the original dynamical core, LWP and cloud fraction decrease when using a longer time step and fewer acoustic sub-steps. This issue is not present with the modified dynamical core. Further, the time-step length can be doubled from 0.5 to 1 s with the new modification, producing virtually the same LWP and cloud fraction, as shown in Figure 22.

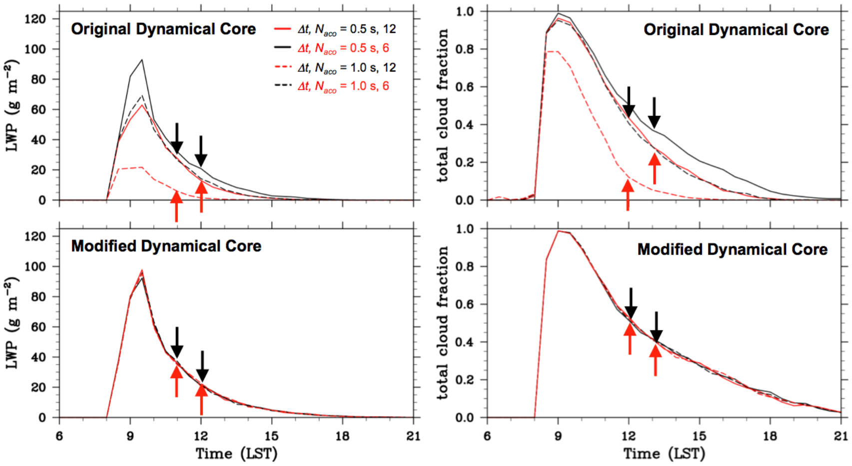

Figure 22. LWP and total cloud fraction from WRF-LES simulations of the 13 May 2008 case with the original (upper) and modified dynamical core (lower) for different time-stepping choices. Arrows highlight sensitivity to *Δt* for a given N_{aco} when changing the dynamical core.

We have also re-run the DRF02 case with the modified dynamical core. The spurious *u* fluctuations do not appear in the simulations using the modified dynamical core (not shown). The convergence problem is also resolved for the DRF02 case, as shown in Figure 23. While the original dynamical core produces different values of LWP, cloud-top/base height, and total cloud fraction for larger and smaller acoustic time steps, the simulations using the modified dynamical core show a convergence for the different acoustic time steps. The modified dynamical core produces cloud fraction that is slightly smaller than the original dynamical core in the final six hours, but the differences between the two dynamical cores are generally small in comparison to the spread of the model ensemble in the first six hours.

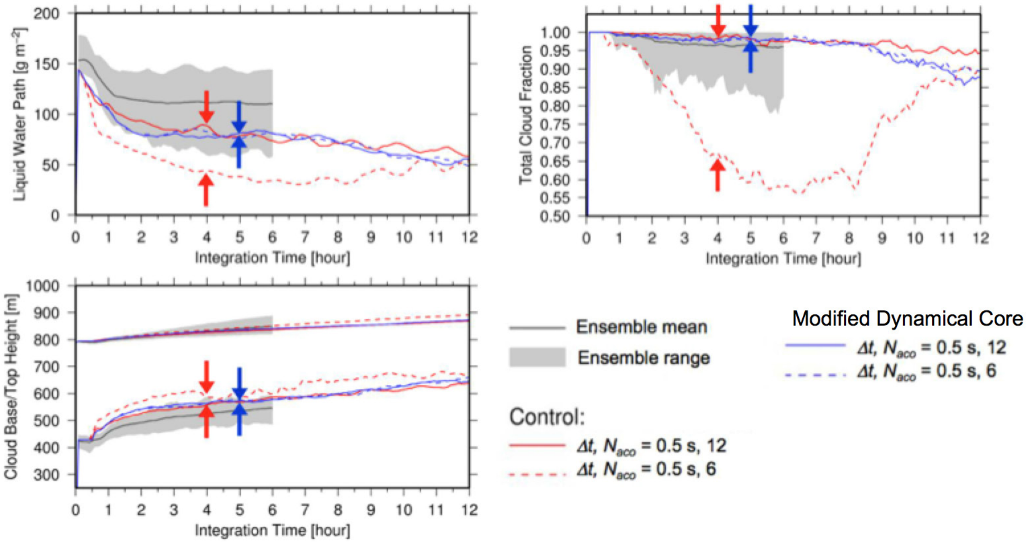

Figure 23. As in Figure 18, except for the sensitivity test using the modified dynamical core for the DRF02 case.

We note that we have not repeated all the sensitivity tests described in Section 2.1 with the modified dynamical core. However, the 13 May 2008 SGP case has a specific humidity jump at the inversion height that is extreme in terms of the climatology of the SGP site, and thus represents a worst-case scenario to test WRF for LES applications. We have performed a sufficient number of relevant simulations, including the extreme case, to indicate the numerical noise has been eliminated so that WRF LES should no longer exhibit time-step convergence issues.

We note that this modification not only addresses the convergence issue, but it also has the added benefit of enabling one to use longer time steps and still yield a converged solution. An initial patch to the model for this modification is being prepared for release in the upcoming WRF v3.7, where it will become available to the community.

3.0 Recommendations

Our team found three methods that can be used to address the convergence issue noted by YF12 in WRF at LES. Each method has its advantages and disadvantages. Our recommendations in order of preference are as follows:

1. modifications to the dynamical core,
2. the WENO advection scheme, and
3. the Galilean transformation.

Option 1 is clearly more desirable over the others since it makes corrections to the governing equations and improves the numerical accuracy of WRF and even improves model’s computational efficiency. In addition, only a few lines of code need to be changed, which will be included in the next release of the code, v3.7 in April 2015. This demonstrates the advantage of a community model, where users and developers can work together and solve problems such as the one in this study. The major outcome of our effort benefits not just ARM and its potential application of WRF for routine LES simulations, but also a large segment of the atmospheric modeling community that uses WRF for basic and applied research. The modifications also permit a larger time step to be used that will reduce the overall computational time needed for simulations, but additional tests are needed to determine how much larger the time step could be without degrading the solution.

Option 2 uses the WENO scheme, and is also an acceptable approach to eliminate the convergence issues in WRF LES. However, we do not know whether the advection scheme does not generate numerical artifacts or whether the advection scheme is filtering or damping noise that is being generated elsewhere within the WRF dynamics. While the Galilean transformation in option 3 is another potential solution, mitigating the numerical noise requires the use of a variable translation wind speed that would need to be computed online for each LES simulation. While this is possible, it is appropriate only for doubly periodic domains, and the numerical noise might erupt sporadically where the transformed wind speed is greatest. The methodology can lower the computational cost by using larger time step. However, it is not the best solution for the convergence issue and additional testing would need to be performed for other LES cases to ensure the veracity of the transformation.

4.0 Summary

With a series of sensitivity simulations, we show the convergence issues (i.e., time-stepping dependency) noted by YF12 occurs when there is a large, specific humidity jump across the inversion at the top of the boundary layer, combined with sufficiently strong wind speed. This study demonstrates the convergence issue is tied to numerical noise generated shortly after the initialization of the simulation, and can occur even before clouds form. Therefore, it is the advection scheme in the dynamical core, rather than the microphysics parameterization or its interaction with the dynamics, produces spurious fluctuations, although dynamics-microphysics interactions may further enhance the fluctuations. The numerical noise stabilizes and does not cause the simulation to crash, but it does lead to enhanced errant vertical mixing at the top of the inversion and reductions in cloud amount.

We have used the long-term measurements from the ARM PBL VAP to show that meteorological conditions predisposing WRF to exhibit the convergence issue occur for ~8% of the SGP radiosondes on average during the year, with greatest frequencies in the spring and summer months. A shortened time step would resolve the time-step convergence issue but can be computationally expensive to robustly cover all the meteorological conditions at the SGP site, so other solutions are sought. We found two methodologies that avoid or minimize the convergence issue: using a Galilean transformation or the WENO advection scheme. When the Galilean transformation or the WENO advection scheme (combined with increased divergence damping) is used, the numerical noise can be avoided or effectively removed and the convergence issue is not present. We found that WENO must be applied to momentum, moisture, and scalars. When WENO is applied to only moisture and scalars, the numerical noise is reduced but not removed entirely. Finally, in collaboration with WRF developers at NCAR, modifications have been made to the dynamics of the model that removes a bug in the code and eliminate the numerical artifacts. The new code does not exhibit the time-stepping dependency and associated convergence issues that exist in previous versions of WRF.

Therefore, we conclude that the numerical issues pointed out in YF12 can be addressed and should not be a factor when considering the use of WRF for routine LES use by ARM.

5.0 References

Ackerman, AS, et al., 2009. “Large-Eddy Simulations of a Drizzling, Stratocumulus-Topped Marine Boundary Layer.” *Monthly Weather Review* 137:1083–1110. DOI:10.1175/2008MWR2582.1.

Blossey, PN, CS Bretherton, M Zhang, A Cheng, S Endo, T Heus, Y Liu, AP Lock, SR de Roode, and K-M Xu. 2013. “Marine Low Cloud Sensitivity to an Idealized Climate Change: The CGILS LES intercomparison.” *Journal of Advances in Modeling Earth Systems* 5:234–258. DOI:10.1002/jame.20025.

Endo, S, AM Fridlind, W Lin, AM Vogelmann, T Toto, AS Ackerman, GM McFarquhar, RC Jackson, and Y Liu. 2015. “RACORO Continental Boundary Layer Cloud Investigations. Part II: Large-Eddy Simulations of Cumulus Clouds and Evaluation with In-Situ and Ground-Based Observations.” *Journal of Geophysical Research*. In revision.

Liu, X, S Osher, and T Chen. 1994. “Weighted Essentially Non-Oscillatory Schemes.” *Journal of Computational Physics* 115:200–212. DOI:10.1006/jcph.1994.1187.

Matheou, G, D Chung, L Nuijens, B Stevens, and J Teixeira. 2011. “On the Fidelity of Large-Eddy Simulation of Shallow Precipitating Cumulus Convection.” *Monthly Weather Review* 139:2918–2939. DOI: http://dx.doi.org/10.1175/2011MWR3599.1.

Moeng, CH, J Dudhia, J Klemp, and P Sullivan. 2007. "Examining Two-Way Grid Nesting for Large Eddy Simulation of the PBL using the WRF Model." *Monthly Weather Review* 135:2295–2311. DOI:10.1175/MWR3406.1.

Ovchinnikov, M, et al. 2014. "Intercomparison of Large-Eddy Simulations of Arctic Mixed-Phase Clouds: Importance of Ice Size Distribution Assumptions." *Journal of Advances in Modeling Earth Systems* 6(1):223–248. DOI: 10.1002/2013MS000282.

Stevens, B, et al. 2005. "Evaluation of Large-Eddy Simulations via Observations of Nocturnal Marine Stratocumulus." *Monthly Weather Review* 133:1443–1462. DOI:10.1175/MWR2930.1.

Van Zanten, MC, et al. 2011. "Controls on Precipitation and Cloudiness in Simulations of Trade-Wind Cumulus as Observed during RICO." *Journal of Advances in Modeling Earth Systems* 3:M06001. DOI:10.1029/2011MS000056.I

Xiao, H, WI Gustafson Jr, and H Wang. 2014. "Impact of Subgrid-Scale Radiative Heating Variability on the Stratocumulus-to-Trade Cumulus Transition in Climate Models." *Journal of Geophysical Research (Atmospheres)*. 119:4192–4203, DOI:10.1002/2013JD020999.

Wang, H, WC Skamarock, and G Feingold. 2009. "Evaluation of Scalar Advection Schemes in the Advanced Research WRF Model using Large-Eddy Simulations of Aerosol-Cloud Interactions. *Monthly Weather Review* 137:2547–2558. DOI:10.1175/2009MWR2820.1.

Wang, H, G Feingold, R Wood, and J Kazil. 2010. "Modelling Microphysical and Meteorological Controls on Precipitation and Cloud Cellular Structures in Southeast Pacific Stratocumulus." *Atmospheric Chemistry & Physics*. 10:6347–6362. DOI:10.5194/acp-10-6347-2010.

Yamaguchi, T, and G Feingold. 2012. "Technical Note: Large-Eddy Simulation of Cloudy Boundary Layer with the Advanced Research WRF Model." *Journal of Advances in Modeling Earth Systems* 4: M09003. DOI:10.1029/2012MS000164.

Appendix A
WRF Configuration for DRF02 Case

We use WRF v3.2.1 for the sensitivity simulations of the DRF02 cases, and WRF v3.6.1 for the simulations testing Galilean transformation, WENO advection scheme, and the modified dynamical core; the two different versions of WRF are in a good agreement in the control simulation. The configuration of the control simulation follows the original case specification by Ackerman et al. (2009). The model domain is 6.4 km × 6.4 km × 1.5 km with 128 × 128 × 200 grid points. The horizontal resolution is 50 m. The vertical grid spacing is stretched (5 m near the surface and inversion; 7.5 m on average). We used simple longwave radiation scheme following the case specification and Lin et al. microphysics scheme modified to include cloud water sedimentation. Surface fluxes and large-scale subsidence are prescribed. The code is compiled with single precision. Details of the model configuration can be found in the "namelist.input" file listed below.

```
&time_control
 run_days                = 0,
 run_hours               = 12,
 run_minutes             = 00,
 run_seconds             = 00,
 start_year              = 2001,
 start_month             = 07,
 start_day               = 11,
 start_hour              = 05,
 start_minute            = 00,
 start_second            = 00,
 end_year                = 2001,
 end_month               = 07,
 end_day                 = 11,
 end_hour                = 17,
 end_minute              = 00,
 end_second              = 00,
 history_interval_m      = 05,
 history_interval_s      = 00,
 frames_per_outfile      = 1,
 restart        =.false.,
 restart_interval_h      = 3,
 io_form_history         = 2
 io_form_restart         = 2
 io_form_input  = 2
 io_form_boundary        = 2
 debug_level     = 0
 io_form_auxinput6       = 2
 auxinput6_inname        = "input_ls_forcing.nc"
 auxinput6_interval_h    = 1
 /
 &domains
```

```
 time_step   = 0,
 time_step_fract_num    = 1,
 time_step_fract_den    = 2,
 max_dom                = 1,
 s_we                   = 1,
e_we                    = 129,
 s_sn                   = 1,
 e_sn                   = 129,
 s_vert                 = 1,
 e_vert                 = 97,
 dx                     = 50,
 dy                     = 50,
 ztop                   = 1500,
 grid_id                = 1,
 parent_id              = 0,
 i_parent_start         = 0,
 j_parent_start         = 0,
 parent_grid_ratio      = 1,
 parent_time_step_ratio = 1,
 feedback               = 0,
 smooth_option          = 0,
 /
 &physics
 mp_physics             = 2,
 ra_lw_physics          = 55,
 ra_sw_physics          = 0,
 radt                   = 0,
 sf_sfclay_physics      = 1,
 sf_surface_physics     = 1,
 bl_pbl_physics         = 0,
 bldt                   = 0,
 cu_physics             = 0,
 cudt                   = 0,
 isfflx                 = 11,
 ifsnow                 = 0,
 icloud                 = 1,
 num_soil_layers        = 5,
 mp_zero_out            = 0,
 /
 &fdda
 /
 &crm
 crm_zsfc               = 0.0,
 crm_lat                = 31.5,
 crm_lon                = -122,
 crm_stretch            = 3,
```

```
 crm_num_pert_layers   = 27,
 crm_pert_amp          = 0.1,
 crm_init_ccn          = 100,
 crm_lupar_opt         = 1,
 crm_znt               = 0.035,
 crm_emiss             = 0.98,
 crm_thc               = 3.,
 crm_mavail            = 0.30,
 crm_force_opt         = 1,
 crm_th_adv_opt        = 0,
 crm_qv_adv_opt        = 0,
 crm_th_rlx_opt        = 0,
 crm_qv_rlx_opt        = 0,
 crm_uv_rlx_opt        = 0,
 crm_vert_adv_opt      = 1,
 crm_num_force_layers = 301,
 crm_flx_opt           = 1,
 crm_sh_flx            = 16,
 crm_lh_flx            = 93,
 crm_albedo_opt        = 1,
 crm_albedo            = 0.1,
 crm_tsk_opt           = 1,
 crm_tsk               = 300,
 crm_ust_opt           = 1,
 crm_ust               = 0.25,
 crm_init_tke_opt      = 1,
 crm_init_tke          = 1.0,
 crm_mp_nc             = 100.,
 crm_num_aer_layers    = 321,
 crm_modlin_opt        = 1,
 crm_sedqc_opt         = 1,
 crm_onlyqc_opt        = 0,
 crm_trans_opt         = 0,
 crm_stat_opt          = 1,
 crm_stat_interval_s   = 10.,
 /
 &dynamics
 rk_ord                = 3,
 diff_opt              = 2,
 km_opt                = 2,
 damp_opt              = 2,
 zdamp                 = 250.,
dampcoef               = 0.01,
 khdif                 = 1.,
 kvdif                 = 1.,
 c_s                   = 0.18
```

```
c_k                    = 0.10
mix_isotropic          = 1
smdiv                  = 0.1,
emdiv                  = 0.01,
epssm                  = 0.1,
tke_heat_flux          = 0.24,
time_step_sound        = 12,
h_mom_adv_order        = 5,
v_mom_adv_order        = 3,
h_sca_adv_order        = 5,
v_sca_adv_order        = 3,
moist_adv_opt          = 1,
scalar_adv_opt         = 1,
momentum_adv_opt       = 1,
mix_full_fields        =.true.,
non_hydrostatic        =.true.,
pert_coriolis          =.true.,
m_opt                  = 1,
/
&bdy_control
periodic_x             =.true.,
symmetric_xs           =.false.,
symmetric_xe           =.false.,
open_xs                =.false.,
open_xe                =.false.,
periodic_y             =.true.,
symmetric_ys           =.false.,
symmetric_ye           =.false.,
open_ys                =.false.,
open_ye                =.false.,
nested                 =.false.,
/
&grib2
/
&namelist_quilt
nio_tasks_per_group     = 0,
nio_groups              = 1,
/
```

Appendix B
WRF Configuration for SGP Case

We use WRF v3.6.1 for the simulations of the SGP cases. The vertical grid spacing is 20 m up to the domain top at 5 km. The horizontal grid spacing is 100 m and the domain size is 25.6 x 25.6 km. We prescribe surface latent and sensible heat fluxes using ARM Best Estimate (ARMBE) dataset. Large-scale forcing was applied to the 14 May 2007 case from the ARM Single Column Model (SCM) Forcing dataset. No large-scale forcing was applied to the 13 May 2008 case as the forcing overly degraded the results for this day. The model is compiled with double precision. Details of the model configuration can be found in the “namelist.input” file listed below.

```
&time_control
 run_days              = 0,
 run_hours             = 15,
 run_minutes           = 00,
 run_seconds           = 0,
 start_year            = 2008,
 start_month           = 05,
 start_day             = 13,
 start_hour            = 12,
 start_minute          = 00,
 start_second          = 00,
 end_year              = 2008,
 end_month             = 05,
 end_day               = 14,
 end_hour              = 03,
 end_minute            = 00,
 end_second            = 00,
 history_interval      = 30,
 frames_per_outfile    = 1,
 auxhist2_interval_s   = 600,
 frames_per_auxhist2   = 18,
 restart               =.False.,
 restart_interval      = 60,
 io_form_history       = 2
 io_form_auxhist2      = 2
 io_form_restart       = 2
 io_form_input         = 2
 io_form_boundary      = 2
 debug_level           = 0
/
&domains
 time_step             = 0,
 time_step_fract_num   = 1,
 time_step_fract_den   = 2,
 max_dom               = 1,
```

```
 s_we                     = 1,
 e_we                     = 257,
 s_sn                     = 1,
 e_sn                     = 257,
 s_vert                   = 1,
 e_vert                   = 251,
 dx                       = 100,
 dy                       = 100,
 ztop                     = 5000,
 grid_id                  = 1,
 parent_id                = 0,
 i_parent_start           = 1,
 j_parent_start           = 1,
 parent_grid_ratio        = 1,
 parent_time_step_ratio   = 1,
 feedback                 = 0,
 smooth_option            = 1
 nproc_x                  = 32,
 nproc_y                  = 16,
 /
&physics
 mp_physics               = 22,
 prong                    = 0,
 ra_lw_physics            = 4,
 ra_sw_physics            = 4,
 radt                     = 1,
 cam_abs_freq_s           = 21600,
 levsiz                   = 59,
 paerlev                  = 29,
 cam_abs_dim1             = 4,
 cam_abs_dim2             = 51,
 sf_sfclay_physics        = 91
 sf_surface_physics       = 0,
 bl_pbl_physics           = 0,
 bldt                     = 0,
 cu_physics               = 0,
 cudt                     = 5,
 isfflx                   = 1,
 ifsnow                   = 0,
 icloud                   = 1,
 num_soil_layers          = 5,
 mp_zero_out              = 0,
 /
 &fdda
 /
&dynamics
```

```
 rk_ord                   = 3,
 diff_opt                 = 2,
 km_opt                   = 2,
 damp_opt                 = 2,
 w_damping                = 0,
 zdamp                    = 500.,
 dampcoef                 = 0.02,
 base_temp                = 290.,
 base_pres                = 100000.,
 base_lapse               = 50.,
 khdif                    = 1.,
 kvdif                    = 1.,
 c_s                      = 0.18,
 c_k                      = 0.1,
 mix_isotropic            = 0,
 smdiv                    = 0.1,
 emdiv                    = 0.01,
 epssm                    = 0.1,
 pert_coriolis            =.true.,
 top_lid                  =.true.,
 tke_heat_flux            = 0.02,
 tke_drag_coefficient     = 0.0013,
 mix_full_fields          =.true.,
 non_hydrostatic          =.true.,
 time_step_sound          = 6,
 h_mom_adv_order          = 5,
 v_mom_adv_order          = 3,
 h_sca_adv_order          = 5,
 v_sca_adv_order          = 3,
 moist_adv_opt            = 2,
 scalar_adv_opt           = 2,
 chem_adv_opt             = 2,
 tke_adv_opt              = 2,
 /
&bdy_control
 periodic_x               =.true.,
 symmetric_xs             =.false.,
 symmetric_xe             =.false.,
 open_xs                  =.false.,
 open_xe                  =.false.,
 periodic_y               =.true.,
 symmetric_ys             =.false.,
 symmetric_ye             =.false.,
 open_ys                  =.false.,
 open_ye                  =.false.,
 nested                   =.false.,
```

```
/
&grib2
/
&namelist_quilt
nio_tasks_per_group    = 0,
nio_groups             = 1,
/
```